

A design and an application of a regional coupled atmosphere-ocean model for tropical cyclone prediction

Henry R. Winterbottom,¹ Eric W. Uhlhorn,² and Eric P. Chassignet³

Received 24 May 2012; revised 28 August 2012; accepted 14 September 2012; published 30 October 2012.

[1] The prediction of tropical cyclone (TC) track has improved greatly in recent decades due in part to the implementation and improvement of numerical weather prediction (NWP) models. However, the prediction of TC intensity using NWP models remains difficult. Several hypotheses have been proposed to explain the factors contributing to the TC intensity prediction errors and one of the leading candidates is the implication of an evolving sea-surface temperature (SST) boundary condition beneath the TC. In this study, a regional scale coupled atmosphere-ocean model is developed using the Advanced Research Weather Research and Forecasting (ARW) model and the HYbrid Coordinate Ocean Model (HYCOM). A coupling algorithm and a methodology to define appropriate ocean initial conditions are provided. Experiments are conducted, during the lifecycle of TC Ike (2008), using both the coupled-model and static (e.g., temporally fixed) SST to illustrate the impacts of the coupled-model for the TC track, intensity, and structure, as well as upon the larger (synoptic) scale. The results from this study suggest that the impact of the evolving SST (e.g., from a coupled atmosphere-ocean model) begin to impact the intensity, size, and thermodynamic structure for TC Ike (2008) at forecast lead-times beyond 48-hours. Further, the forecast trajectories (i.e., tracks) do not illustrate large differences between the non-coupled and coupled-models. Finally, the impact of the SST boundary condition upon TC Ike (2008) appears to be a function of the strength of the atmospheric forcing – in particular the size and intensity of the TC wind field.

Citation: Winterbottom, H. R., E. W. Uhlhorn, and E. P. Chassignet (2012), A design and an application of a regional coupled atmosphere-ocean model for tropical cyclone prediction, *J. Adv. Model. Earth Syst.*, 4, M10002, doi:10.1029/2012MS000172.

1. Introduction

[2] The forecast skill for tropical cyclone (TC) position (e.g., track) has increased in recent decades (see NHC Tropical Cyclone Forecast Verification available at <http://www.nhc.noaa.gov/verification>, hereinafter referred to as NHC Tropical Cyclone Forecast Verification). This improvement has been attributed, at least in part, to the use and ongoing development of the numerical weather prediction (NWP) models which are utilized by the National Hurricane Center (NHC) and other weather agencies when issuing forecasts. Despite the improvement for TC track predictions, similar improvement trends are

not seen when evaluating the skill relative to TC intensity forecasts (NHC Tropical Cyclone Forecast Verification). Several hypotheses have been proposed to explain the intensity forecast difficulties. In particular, much emphasis has been placed on the ocean boundary condition within NWP models – specifically those NWP models tasked with producing TC track and intensity forecasts (e.g., HWRF). Currently, the majority of the global operational NWP models employ a static (i.e., non-temporally evolving) sea-surface temperature (SST) boundary condition. A consequence is that the TC's impact upon the upper ocean and the upper ocean mixed-layer (OML) is not simulated and thus the OML does not evolve in accordance with the forcing induced by the TC [Price, 1981; Brooks, 1983; Bender and Ginis, 2000; Shay et al., 2000; Chan et al., 2001].

[3] In recent years regional-scale NWP models, specifically those applied for TC prediction, have implemented *interactive* ocean boundary conditions. Bender and Ginis [2000] discuss the coupling of the Princeton Ocean Model (POM) [Blumberg and Mellor, 1987] to the high resolution Geophysical Fluid Dynamics Laboratory (GFDL) TC prediction model [Kurihara et al., 1993]. More recently, the next generation operational TC prediction

¹Cooperative Institute for Research in Environmental Studies, National Oceanic and Atmospheric Administration, Earth System Research Laboratory, Boulder, Colorado, USA.

²Hurricane Research Division, National Oceanic and Atmospheric Administration, Atlantic Oceanographic and Meteorological Laboratory, Miami, Florida, USA.

³Center for Ocean-Atmospheric Prediction Studies, Florida State University, Tallahassee, Florida, USA.

model – the Hurricane Weather Research and Forecasting (HWRF) model, has been coupled to the POM and a *feature-based data assimilation* (FBDA) methodology [Falkovich *et al.*, 2005; Yablonsky and Ginis, 2008] has been implemented in order to better diagnose the position and the magnitude of the TC induced oceanic cold-wake within the SST analysis. Despite these advances in TC modeling efforts, much research (and thus modeling) remains to be done in order to better understand the physics of the air-sea interactions within TCs. Much has been learned through observations [Powell *et al.*, 2003; Chen *et al.*, 2007; Zhang *et al.*, 2009; Zhang, 2010] and some of this knowledge has been implemented within NWP models [Bao *et al.*, 2000; Moon *et al.*, 2004; Nolan *et al.*, 2009a, 2009b]. However without easily accessible tools to study such phenomena within a NWP model reference frame, the incorporation of any knowledge gained from observational studies becomes nearly impossible.

[4] It is not the intention of this study to highlight and/or identify the pitfalls of the current NWP methods (involving coupled-models) for TC prediction. Rather, we provide the reader an easily accessible methodology for coupling independent geophysical (specifically atmosphere and ocean) models. The algorithms provided within may be extended such that other pertinent geophysical prediction (e.g., wave and sea-spray) models may be coupled with those for the atmosphere and ocean. The impact of the coupled-model for both the TC and the larger (synoptic) scales is illustrated using NWP forecast experiments conducted during the life-cycle of TC Ike (2008). The remainder of the manuscript is organized as follows. In section 2 we discuss the atmosphere and ocean model coupling methodologies while section 3 describes the experiment configurations for TC Ike (2008) as well as the TC tracking and diagnostic variable evaluation algorithms. In section 4 we analyze the results from each of the experiments and conclude (in section 5) with both a discussion of and possible applications for future studies.

2. Methodology

[5] This section describes the details of the coupled-model and the TC detection and diagnosis algorithms. The atmosphere and ocean model physics, listed in Table 1, are identical for all experiments.

2.1. Coupled Atmosphere-Ocean Model Description

[6] Version 2 of the Advanced Weather Research and Forecasting (ARW) model [Skamarock *et al.*, 2005] provides the atmosphere model for the coupled modeling

system. The ARW is a fully compressible, non-hydrostatic model using a dry-hydrostatic terrain-following vertical coordinate (η). The model dynamics evolve from a flux-form of the Euler equations (following Ooyama [1990]) and are integrated forward using a 20-second time-step and the 3rd order Runge-Kutta time-stepping scheme described by Wicker and Skamarock [2002]. The Mercator projected ARW domain has a horizontal grid spacing of 7.810-km and is centered at 28.58N, 55.4W while the vertical coordinate consists of 36-unevenly spaced η -levels.

[7] The HYbrid Coordinate Ocean Model (HYCOM; v90.3) [Bleck, 2002; Chassignet *et al.*, 2003; Halliwell, 2004] simulates the oceanic forcing within the coupled modeling system. The appeal of HYCOM is the behavior of the model vertical coordinate: (a) within stratified ocean regions, HYCOM’s vertical coordinate is defined using target densities (or isopycnals); (b) within shallow coastal regions the coordinate transitions to a terrain (e.g., ocean bathymetry) following coordinate (i.e., σ); (c) finally in un-stratified seas and the OML the vertical coordinate transitions to a z -level (or height) coordinate. The target density isopycnals are identical to those of the Naval Oceanographic Office (NAVOCEANO) global HYCOM experiment 90.3 configuration. Additional details regarding the characteristics of the HYCOM vertical coordinate may be found in Chassignet *et al.* [2003, and references therein]. The HYCOM horizontal grid is a sub-region of the $1/12$ degree (approximately 8.81-km) NAVOCEANO global HYCOM.

[8] The attributes for the respective ARW and HYCOM grids are summarized in Table 2. We note that the dimensions of the ARW grid are larger than that of the ocean model to ensure that there exist atmospheric forcing variables for each HYCOM grid cell. However, this also means that the atmosphere and ocean model grids are not exactly co-located. When the offset between the grids is small, the error introduced when interpolating the atmospheric forcing from the ARW horizontal grid to the HYCOM horizontal grid is small. This is the case for all experiment configurations presented in this study. However, as the offset between the respective model’s grid spacing increases, the potential for interpolation error increases. In these instances, more advanced interpolation schemes, such as those described in Press *et al.* [1992], are desired. However, for this study a simple bi-linear interpolation scheme is applied when coupling ARW and HYCOM. Figure 1 illustrates the ARW and HYCOM coupled-model domain as well as the observed track for the TC Ike (2008) case study.

Table 1. The Relevant Atmosphere (ARW) and Ocean (HYCOM) Model Physics Parameterizations for all Experiments in This Study

Physics Parameterization	Long-Wave Radiation	Short-Wave Radiation	Micro-physics	Planetary-Boundary-Layer	Cumulus Convection	Ocean Mixed-Layer
Scheme	Rapid Radiative Transfer Model (RRTM)	Dudhia	Lin <i>et al.</i> ,	Mellor-Yamada-Janjic turbulent kinetic-energy (TKE)	Betts-Miller-Janjic	K-profile (KPP)

Table 2. The Atmosphere (ARW) and Ocean (HYCOM) Model Configurations

Model	Atmosphere (ARW)	Ocean (HYCOM)
Grid-spacing Resolution	7.81-km	1/12° (8.81-km at the equator)
Grid Dimension (X × Y × Z)	1074 × 549 × 35	1063 × 545 × 32
Time-step	20-seconds	300-seconds (baroclinic) 10-seconds (barotropic)

[9] The algorithm to couple ARW and HYCOM is as follows:

[10] 1) ARW integrates from $t=t_0$ to $t=t_0+dt$ where t is the model time, t_0 is the initial time at the coupling interval, and dt is the coupling interval; this provides the atmospheric variables required to force HYCOM

[11] 2) The atmosphere variables for 10-meter wind, 2-meter temperature, 2-meter mixing ratio, and precipitation rate are interpolated to the HYCOM horizontal grid; the zonal- and meridional wind stress vectors are then computed using the NAVOCEANO HYCOM formulation [Kara *et al.*, 2000]

[12] 3) HYCOM integrates within the same time interval (i.e., $t=t_0$ to $t=t_0+dt$) and provides an updated SST which is then interpolated to the ARW grid

[13] Because the HYCOM grid is smaller than the ARW grid, the SST values beyond the edges of the HYCOM domain are not updated and as a result are held fixed for the duration of the forecast. Figure 2 provides a flowchart for the coupling described above. We note that the possibility exists to include additional geophysical models (i.e., WAVEWATCH-3) [Tolman, 1999] within the existing coupled-model system. However, these efforts are beyond the intent of the simple methodology described in this study.

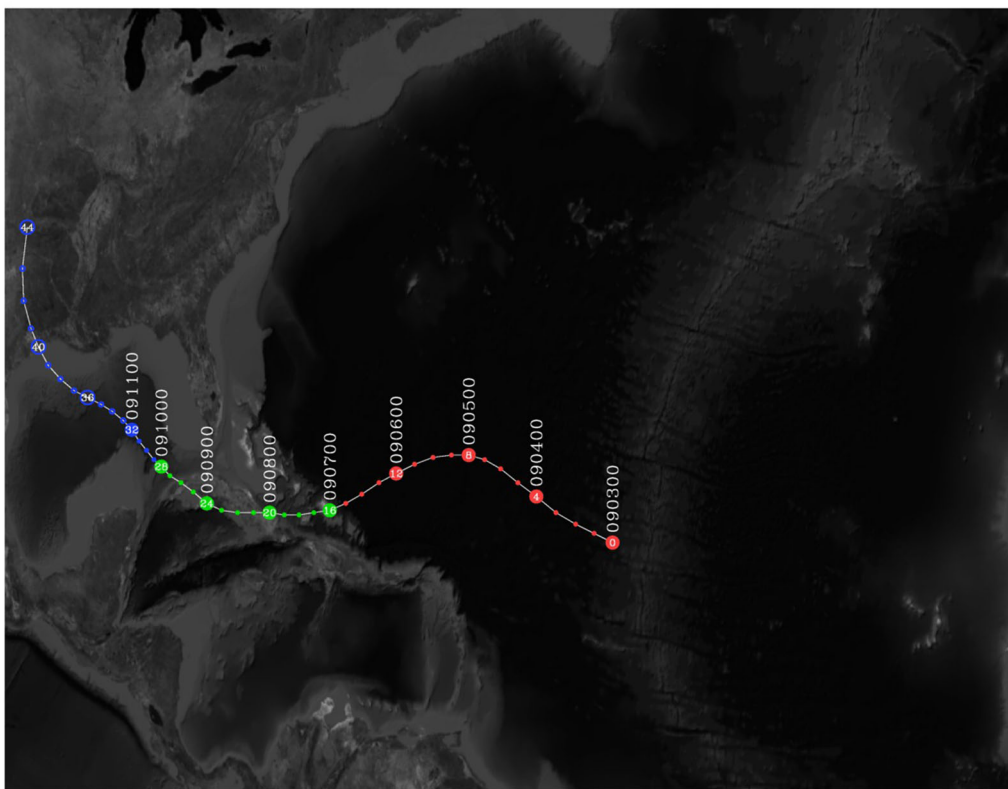


Figure 1. The co-located atmosphere (ARW) and ocean (HYCOM) model grids. The ARW terrain field is computed from a 30-arc second topography while the ocean bathymetry is computed from the 2-minute Digital Bathymetric Data Base (DBDB2) and is identical to a similar region within the NAVOCEANO global HYCOM (v90.3). The re-analysis positions for TC Ike (2008) are illustrated by the super-imposed track. The dates, formatted as MMDDHH, are provided a 6-hour intervals beginning 0000 UTC 03 September. The solid circles indicate the dates when experiments are launched while the open circles indicate when only model forecasts are available. The red, green, and blue circles indicate the different time-periods referenced throughout the manuscript for TC Ike. The co-located regions extend from approximately 94W, 8N to 11W, 46N.

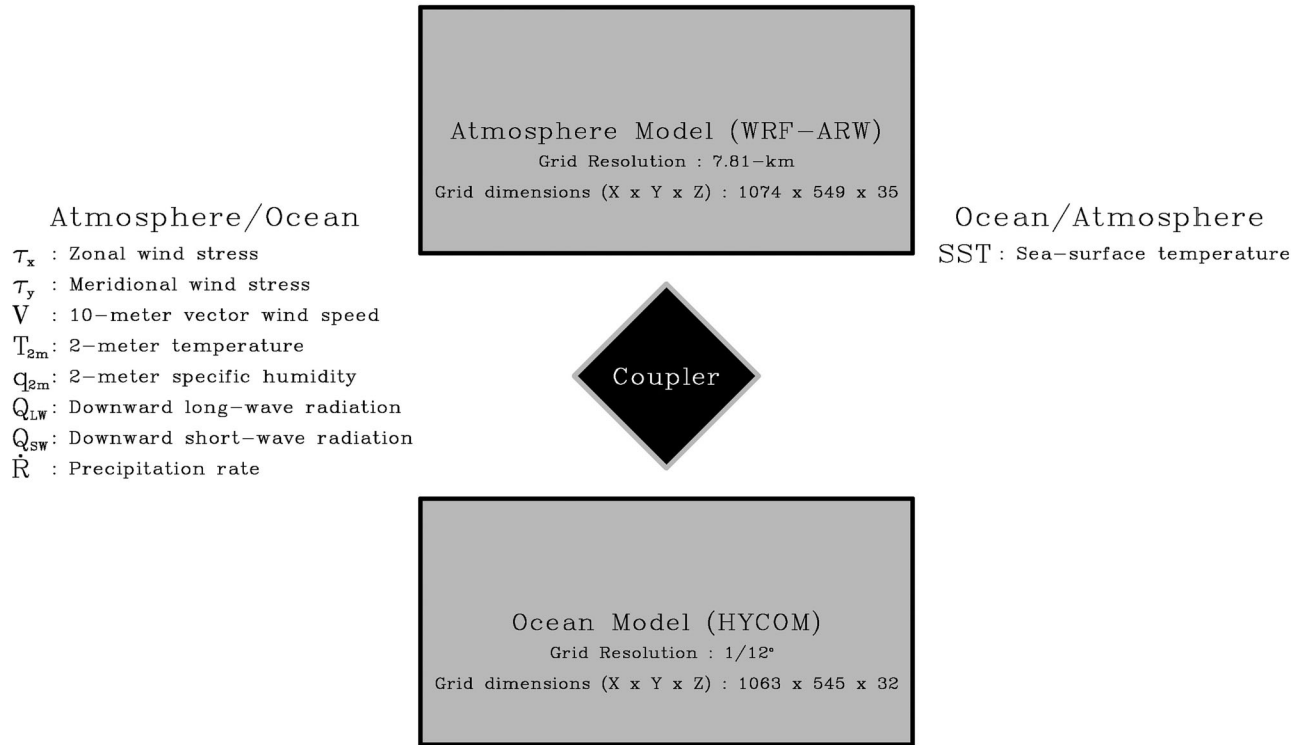


Figure 2. The coupled-modeling algorithm for the experiments comprising this study. During a coupled-model experiment, the atmosphere model (ARW) integrates forward in time and the atmosphere variables are interpolated to the ocean model (HYCOM) simulation grid in order to provide temporally varying forcing. At the end of the coupling interval (i.e., 30-minutes), the updated SST (provided by HYCOM) is interpolated to the ARW simulation grid and the process continues and then repeats at the next model coupling time.

2.2. Atmosphere Model Initial Conditions

[14] The ARW initial and lateral boundary conditions are provided by the National Centers for Environmental Prediction (NCEP) Final Analysis (FNL). These analyses are derived from the NCEP Global Forecast System (GFS) spectral and data assimilation forecast model. The NCEP-GFS configuration to compute the NCEP-FNL is run 3-hours past the synoptic time permitting the assimilation of additional observations. The resolution of the NCEP-FNL analyses is $0.5^\circ \times 0.5^\circ$ and defined on 26 isobaric levels. The only concession made for TCs within the NCEP-FNL analysis is the vortex relocation scheme discussed by Lord [1991]. We note that synthetic (i.e., bogus) TC vortex methods are not implemented for the NCEP-GFS.

2.3. Ocean Model Initial Conditions

[15] For experiments using a SST analysis (e.g., HYCOM) that is different from the SST analysis within the atmosphere model initial conditions, care should be taken such that the SST and OML are balanced with respect to the atmospheric forcing. In doing so, the discontinuities resulting from oceanic and atmospheric fluxes (within the respective boundary layers) will be reduced and thus eliminating adjustments that may be non-physical. For this study we addressed this by first obtaining and interpolating the NAVOCEANO HYCOM ocean analysis, valid at a date 5-days (120-hours) prior to the

respective experiment date, to the HYCOM simulation grid. Next, a 5-day (120-hour) ocean *spin-up* forecast is launched where the HYCOM atmospheric forcing variables are computed from the atmospheric analysis that will define the horizontal and lateral boundary conditions for ARW, in this case the NCEP-FNL. At the end of the spin-up period, the HYCOM SST and OML states approach an approximate balanced state with respect to the NCEP-FNL analysis. For the models (i.e., ARW and HYCOM) and the analyses (i.e., NCEP-FNL and NAVOCENO) chosen for this study, this step becomes necessary since the HYCOM Ocean Prediction System [Chassignet *et al.*, 2007, 2009] computes the NAVOCEANO HYCOM atmospheric forcing from the corresponding Navy Operational Global Atmospheric Prediction System (NOGAPS) atmospheric analysis and as a result, large oscillations within the OML mean kinetic energy time-series are observed – particularly early on in the SST analysis spin-up phase.

[16] Figure 3 illustrates the OML mean kinetic energy (KE) time-series (red line), the standard deviation about the mean KE (black boxes), and the minimum and maximum KE values (gray whiskers) for the 33 HYCOM experiments (discussed in section 3) during the lifecycle of TC Ike (03 September – 11 September, 2008). During the HYCOM spin-up period and prior to the respective experiment’s initialization (e.g., negative forecast hours), the mean KE time-series illustrates large oscillations suggesting the presence of imbalances resulting from the different atmospheric

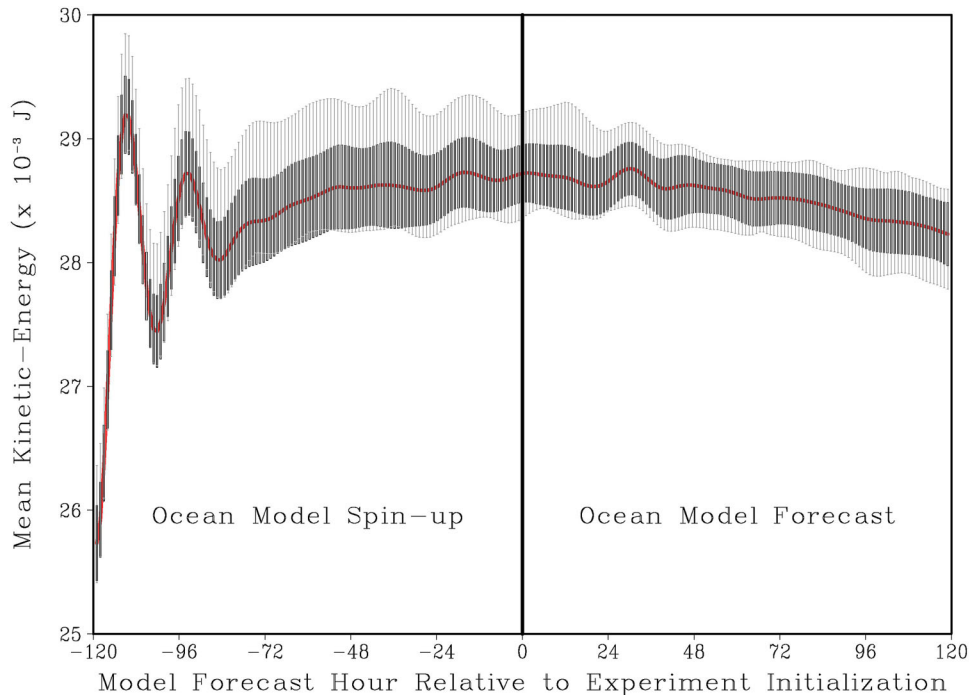


Figure 3. The mean OML KE (red line) computed from each HYCOM SST experiment. The black boxes indicate ± 1 -standard deviation about the mean. The error bars (gray whiskers) illustrate the range (i.e., minimum and maximum values) computed from all (e.g., 33) experiments. The *ocean model spin-up* corresponds to the 120-hour pre-forecast period when the ocean state is adjusted toward the NCEP FNL analysis. The subsequent HYCOM model forecast (i.e., ocean model forecast) begins from the ocean state that has been spun-up with respect to the atmosphere model (e.g., ARW) model analysis. The vertical black line indicates the end of the *ocean model spin-up* phase and the beginning of the *ocean model forecast*.

analyses. The atmospheric forcings derived from the NCEP-FNL, namely the precipitation rate, the magnitude and direction of the wind-stress forcing, and the resulting heat and moisture fluxes, are different from those computed from the NOGAPS analyses. Following the 5-day period, the oscillations have been considerably reduced suggesting a restoration of balance between the ocean and atmosphere initial states. As a result the *ocean model forecast* begins from a state with very small oscillations in the KE spectrum. It is worth noting that the 120-hour spin-up period may be more than is required for the TC Ike (2008) experiments. However, *Winterbottom* [2010] illustrated and documented instances when the large KE spectrum oscillations occurred beyond the 120-hour spin-up as a result of modifications (e.g., synthetic treatment) for the analysis TC vortex during the simulation period. In order to remain consistent with the previous study, we proceed with the methodology prescribed by *Winterbottom* [2010]. By retaining the 120-hour pre-forecast spin-up period we note that the main drawback is the use of computational resources and that the main improvement is an ocean model state that is approaching a more balanced state with respect to the atmosphere model initial conditions.

2.4. Tropical Cyclone Detection and Structural Diagnosis

[17] In order to illustrate the impact of the SST upon the TC and the synoptic (e.g., environmental) scales, an

algorithm is employed to detect and compute the position, the intensity, and the TC structural attributes. This algorithm is composed of and derived from the methods discussed by *Marchok* [2002], *Liu and Chan* [1999], *Hart* [2003], *Kimball and Mulekar* [2004], and *Powell and Reinhold* [2007].

[18] The first-guess position provided to the NCEP TC tracking algorithm [*Marchok*, 2002] is obtained from the extended best-track reanalysis [*Demuth et al.*, 2006]. The *forecasted* geographical positions are determined by searching a radial region, defined by a climatologically estimated maximum TC movement distance during successive forecast times (187-km for this study), for the minimum sea-level pressure location. Once this location is determined, the *Marchok* [2002] algorithm is again implemented to compute the consensus position for the TC. We note that although it is possible for *non-TC* sea-level pressure minima to be identified as *forecasted* TC positions, the results (discussed in section 4) suggest that the methodology employed in this study during the lifecycle of TC Ike (2008) is sufficient.

[19] Once the TC position is identified, the intensity, size, and TC thermodynamic structure metrics are computed. The maximum wind speed intensity, V_{\max} , and the radius of maximum wind (RMW) are estimated as follows. We first locate the maximum 10-meter wind speed within a 150-km radius. The 150-km radius is chosen based on the climatological values provided in

Kimball and Mulekar [2004]. The V_{\max} is the largest 10-meter wind speed magnitude within the aforementioned 150-km radius and the RMW is the radius at which the respective V_{\max} occurs. The minimum sea-level pressure (MSLP) intensity is the minimum value for the sea-level pressure within the 150-km radius. The radius of the TC circulation (ROC) is estimated using the relative vorticity criteria discussed in Liu and Chan [1999].

[20] The integrated kinetic energy (IKE) is computed from the formulation described in Powell and Reinhold [2007] using all TC relative wind speed magnitude values greater than or equal to 17 m s^{-1} within the ROC estimated above. Finally, the cyclone phase space (CPS) parameters, namely the lower ($-V_T^L$) and upper ($-V_T^U$) troposphere thermal wind parameters are calculated as discussed in Hart [2003].

3. Experiment Configurations

3.1. Brief Synoptic History for TC Ike (2008)

[21] A tropical wave that quickly moved across the Atlantic Ocean intensified to a tropical depression, shortly thereafter intensified to a tropical storm and maintained that intensity into early 03 September when the storm was designated TC Ike (2008). TC Ike underwent a subsequent intensification and reached a peak intensity of 125-kts on 04 September and was thus classified as a Saffir-Simpson category 4 hurricane. TC Ike continued its general westward movement during 05 and 06 September while slowly weakening in the presence of environmental shear before subsequently (once again) intensifying to a Saffir-Simpson category 4 Hurricane on 07 September as it passed over the Turks and Caicos Islands. Later on 07 September, TC Ike made its first Cuban landfall as a category 4 TC and weakened before making a second Cuban landfall as a category 1 hurricane on 09 September. TC Ike then moved into the Gulf of Mexico and made its final landfall near Galveston, Texas USA as a category 2 hurricane [Berg, 2009]. The best-track reanalysis positions for TC Ike, beginning 0000 UTC 03 September and ending 0000 UTC 14 September, are provided in Figure 1 at 6-hourly intervals. The positions shaded in red are the times when TC Ike was over the Atlantic Ocean basin waters while the positions shaded in green indicate when TC Ike was either making its repeated landfalls and/or was in close proximity to land. Finally, the blue shaded positions indicate the times when TC Ike was in the Gulf of Mexico and leading up to TC Ike's final landfall near Galveston, Texas U.S.A.

4.2. Control Experiments

[22] The control experiments (CNTRL) for TC Ike (2008) begin 0000 UTC 03 September and continue four-times daily until 0000 UTC 11 September. The result is 33 experiments each initialized at 6-hour intervals. The initial and lateral-boundary conditions for the ARW model are computed from the NCEP-FNL. Each experiment produces a 72-hour forecast with 3-hourly model output. The SST is held fixed (i.e., does not evolve in response to the atmospheric forcing) for the

duration of the forecast and is defined by the HYCOM model SST resulting from the spin-up procedure discussed in section 2.

4.3. Coupled-Model Experiments

[23] The coupled-model experiment (EXPT) atmosphere initial conditions are defined by the NCEP-FNL analyses while the SST *initial* condition is identical to that of CNTRL. The SST is permitted to evolve according to the ARW forcing and the HYCOM dynamics and is updated at 30-minute intervals using the results from the HYCOM integration at the coupling interval. The duration and output intervals for EXPT are also identical to CNTRL.

4. Experiment Results

[24] In this section, we present the results from each of the experiments designed to evaluate the sensitivities of TC track, intensity, structure and also the synoptic-scale (environmental) predictors as a function of the SST boundary condition.

4.1. Tropical Cyclone Track Predictions

[25] Figure 4 illustrates the position error for TC Ike (2008), relative to the best-track reanalysis position for CNTRL and EXPT. The results are provided as a function of (a) 24-, (b) 48-, and (c) 72-hour forecast lead-times relative to the forecast initialization time denoted within the color bar. The radial distance (gray) contours are drawn at 100-km intervals beginning with 100-km. The symbols defining the respective CNTRL and EXPT experiment forecast positions are designated within the figure legend while the mean track position (distance) error for CNTRL and EXPT (respectively) are provided above each panel. Finally, the mean distance error from CNTRL and EXPT and the NHC, at the respective forecast lead-time, are illustrated by the solid and dashed white contours, respectively.

[26] The forecast lead-time differences between CNTRL and EXPT are small for all experiments illustrated in Figure 4. However, the differences with respect to the observed track position increase as functions of forecast lead-time and forecast initialization time. The track errors during the early period of TC Ike's lifecycle (red positions in Figure 1), particularly prior to the first Cuban landfall (denoted by the green positions in Figure 1), are large relative to those experiments when the TC arrives within the Gulf of Mexico (blue positions in Figure 1). We note that these experiments (0 through 15 from Figure 1) were initiated with NCEP-FNL analyses containing a very weak TC vortex. Comparatively speaking, these experiments have a larger forecast position error when compared to the experiments initialized with an NCEP-FNL analysis initial condition that has a stronger initial TC vortex. These results do not suggest that there exist deficiencies within the ARW atmospheric dynamics. Rather these results suggest that the uncertainties associated with the structure and intensity (see Figure 5) of TC Ike, within the NCEP-FNL and ARW versus the structure and intensity of the observed event, enable the simulated TC

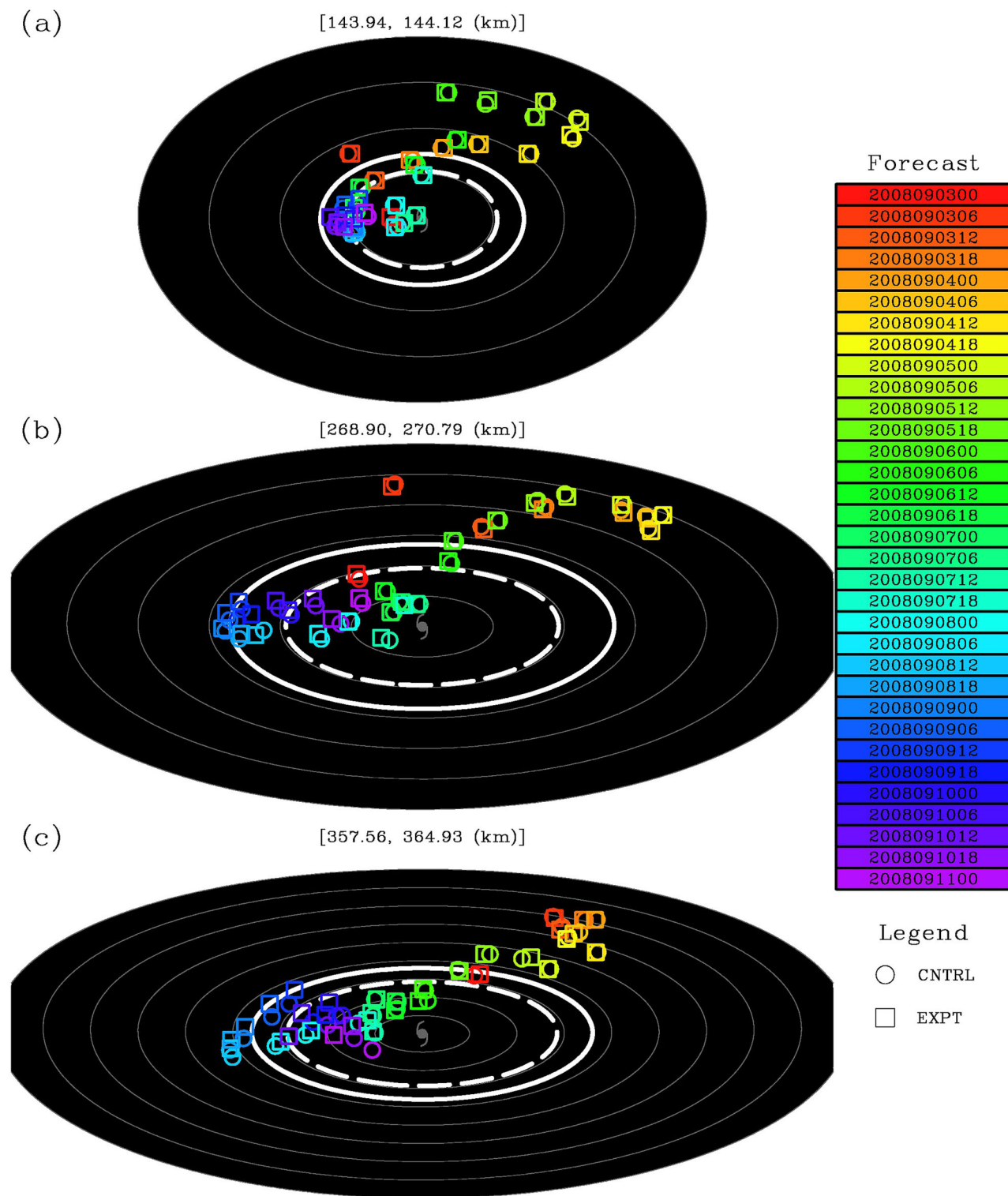


Figure 4. Along track position forecast errors (indicated in the legend) as a function of forecast lead-time: (a) 24-hours, (b) 48-hours, and (c) 72-hours. The mean forecast error is provided above each figure panel for CNTRL and EXPT, respectively. The radial contours (gray), relative to the observed (i.e., best-track reanalysis) TC position are drawn at 100-km intervals beginning at 100-km. Finally, the solid white line indicates the mean forecast error computed from CNTRL and EXPT at the respective lead time while the dashed white line is the NHC official mean forecast error for the respective forecast lead-time.

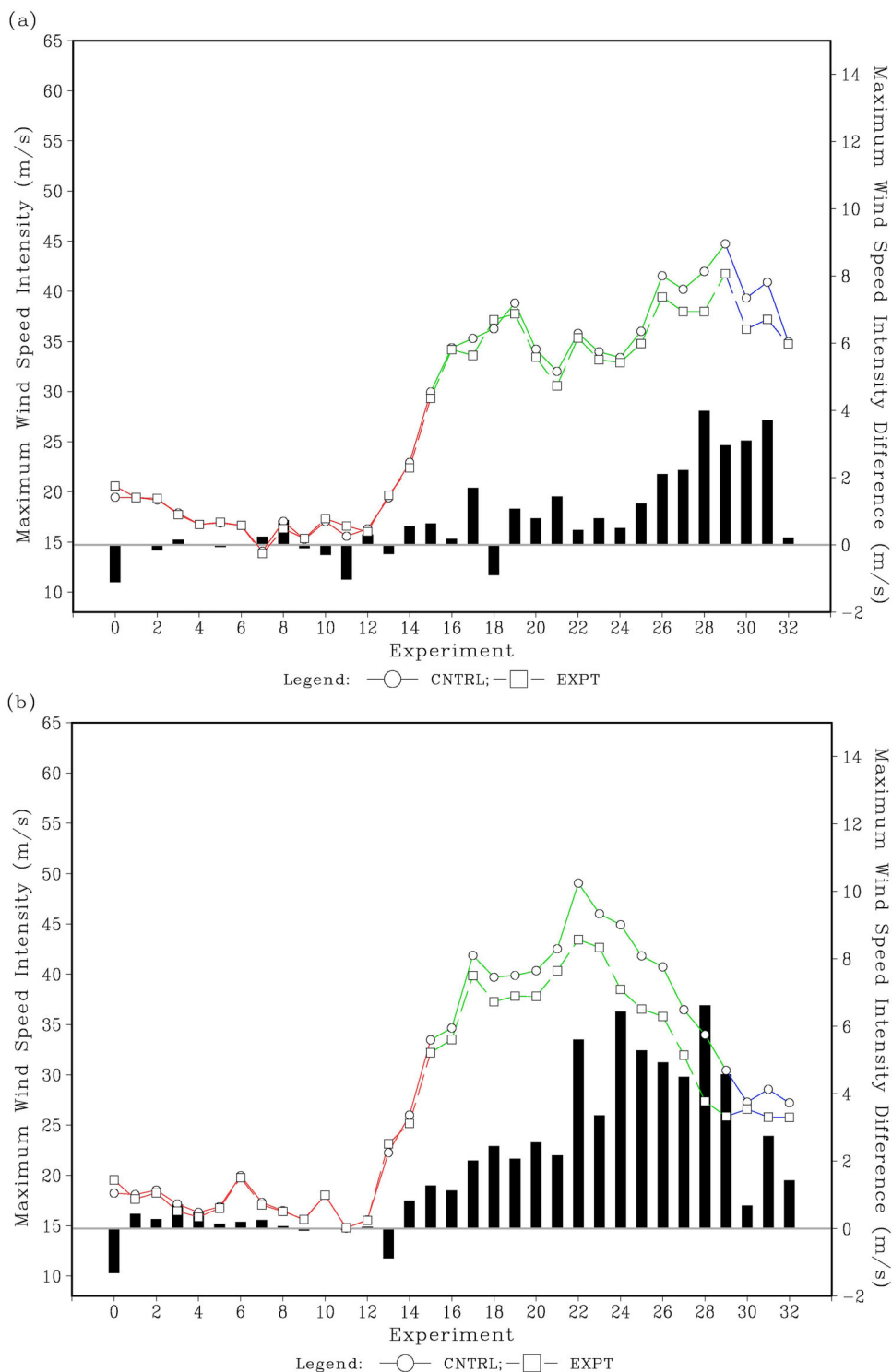


Figure 5. TC Ike (2008) maximum wind speed intensities as a function of forecast lead-time ((a) 24-hours, (b) 48-hours, and (c) 72-hours) for the experiment configurations denoted within the legend. The colors and the experiment numbers (along the x-axis) are identical to those illustrated in Figure 1. Finally, the black histogram bars indicate the difference between CNTRL and EXPT experiments (i.e., CNTRL – EXPT).

vortex to be advected by different environmental steering components. The implications of environmental steering are discussed in *Pike* [1985], *Dong and Neumann* [1986], *Velden and Leslie* [1991], and *Elsberry*

[1995]. Further, the above results do not implicate the SST boundary conditions as the leading order mechanism by which the respective forecasts vary. These results do suggest that the SST boundary condition

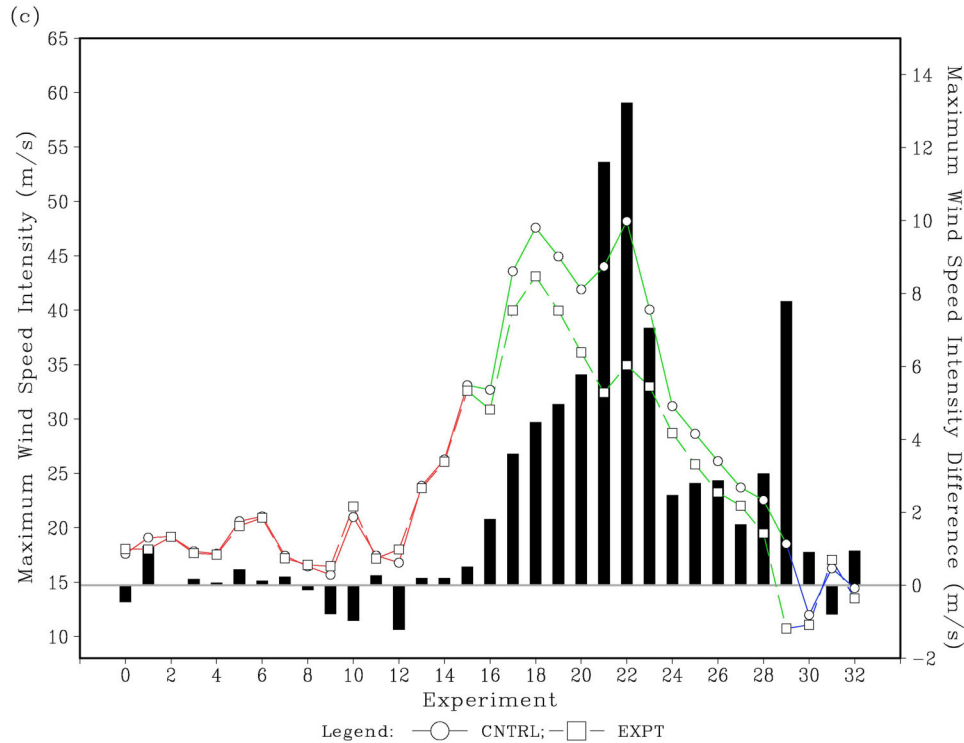


Figure 5. Continued.

(and its associated uncertainties) may influence the response of the respective atmosphere model physics – namely the boundary layer parameterizations. The feedbacks between the respective parameterization schemes may lead to different intensities and thus ultimately different TC trajectories. Although the synoptic-scale forcing seems as though it is the primary mechanism governing the different forecast track predictions for TC Ike (2008), we cannot discount the predictability limits (or lack thereof) related to the non-linear characteristics and interactions within the ARW atmosphere model.

4.2. Tropical Cyclone Intensity Predictions

[27] Figure 5 provides the CNTRL and EXPT V_{\max} intensities (as indicated within the legend) and the V_{\max} differences (CNTRL – EXPT; black bars) for TC Ike (2008) as a function of (a) 24-, (b) 48-, and (c) 72-hour forecast lead-times. The experiment numbers correspond to those in Figure 1. The V_{\max} intensities suggest that the impact of the SST boundary condition becomes more influential as the simulated TC vortex becomes more intense. When the ARW TC is weak and/or when TC Ike (2008) is within shallow ocean regions (experiments 1–15), there is little variability between CNTRL and EXPT. This may be in part due the behavior of the HYCOM vertical coordinate in shallow oceanic regions [see Bleck, 2002; Chassignet et al., 2003, and references therein]. However, as TC Ike approaches Cuba (see experiments 16–17; green positions), the agreement between the observed and the respective CNTRL and EXPT experiments improves. Finally, as TC Ike (2008)

enters the Gulf of Mexico (blue positions), the observed and experiment V_{\max} intensities continue to improve.

[28] In nearly all instances, the CNTRL experiment has a stronger TC at each lead-time. This is particularly true when the TC is nearing and the influence of the terrain of Cuba and when TC Ike (2008) enters the Gulf of Mexico. This result may be attributed to the interaction of the ARW parameterized boundary-layer physics with the temporally varying HYCOM SSTs for EXPT. The track positions for CNTRL when V_{\max} is more intense than EXPT coincide with the position of the warmest SSTs in the Gulf of Mexico. This suggests that the interaction of the ARW boundary-layer physics parameterization (e.g., YSU) with the non-varying SST may lead to a stronger simulated TC. This is consistent with the findings of Bender and Ginis [2000] and suggests that the intensity variability is due to the interaction of the SST boundary condition with the ARW physics. Although the simulated TC intensity is weaker than the observed V_{\max} (likely due to several NWP model factors including spatial resolution and incomplete physical parameterizations), the results are thermodynamically valid when describing a TC from theoretical principles (see Emanuel [1986]) while also consistent with the behavior of observed TCs [Cione and Uhlhorn, 2003]. The CNTRL (i.e., non-evolving) SST is warmer than the EXPT SST and therefore provides a greater source of energy for the TC. The warmer SST boundary condition leads to a larger flux of sensible and latent heat into the atmosphere boundary layer and provides a mechanism for sustained deep convection resulting from the enhanced atmospheric instability.

[29] Finally, these results seem to indicate that although the SST boundary-condition has a small impact upon the motion of the TC (as discussed in the previous section and illustrated in Figure 4), the evolution of the SST boundary-condition (specifically EXPT) does introduce an additional uncertainty into the prediction of the V_{\max} intensity, in particular at longer (e.g., 48- to 72-hour) forecast lead times. These results are consistent with previous numerical modeling [Chan *et al.*, 2001] and observational [Hong *et al.*, 2000] studies which have diagnosed a TC's intensity response to SST variability.

4.3. Tropical Cyclone Thermodynamic Structure Predictions

[30] The CPS [Hart, 2003] ($-V_T^L$) versus ($-V_T^U$) parameters computed from CNTRL and EXPT, at (a) 24-, (b) 48-, and (c) 72-hour forecast lead-times, are illustrated in Figure 6. The differences between the CNTRL and EXPT (e.g., CNTRL – EXPT) as a function of experiment are provided in the respective inset figures. It is worth noting that there exists an unavoidable, albeit small, amount of uncertainty due to the TC vortex position algorithm [Marchok, 2002]. However, this is only of concern when the NCEP-FNL analysis and/or ARW representation for TC Ike (2008) is weak. Although this is the case during the experiments from 03 September through 06 September, we will consider this a negligible source of uncertainty.

[31] For 24-hour forecast lead-times (Figure 6a), the CPS results suggest that the TC Ike (2008) tropospheric thermodynamic structure is largely insensitive to the temporal (and thus spatial) variability within the SST boundary condition. The small bifurcations between CNTRL and EXPT for experiments 30 through 33 are a result of geographical position differences and the interaction of TC Ike's circulation with topography.

[32] At lead-times of 48-hours (Figure 6b), the inter-comparisons for ($-V_T^L$) and ($-V_T^U$) remain in general agreement for experiments 1 through 21. The divergence in solutions for experiments 22 through 30 is likely, once again, an artifact of the small differences in simulated TC position (see Figure 4) and the respective TC's interaction with Cuba's topography. At a 48-hour forecast lead-time, TC Ike's troposphere thermodynamic structure appears to remain insensitive to the different SST boundary conditions.

[33] For lead-times of 72-hours (Figure 6c) the difference in solutions is more apparent as the simulated TC becomes more intense (i.e., experiments 17 through 33). We cannot, once again, discount the influence of TC position and topographical effects on the CPS parameter values. However, in EXPT where the SST is varying in time, the trajectory describing the depth of the tropospheric warm core (through the CPS) becomes quite different for experiments 17–33. Each of the 72-hour forecast positions is in general agreement (see Figure 4) suggesting that the evolution of the SST boundary conditions is contributing to the different CPS states for TC Ike (2008).

[34] From the CNTRL and EXPT experiments presented in this study it is difficult to conclude the mechanisms (e.g., air-sea interactions, suppression of convection, etc.) responsible for the CPS differences, particularly at longer lead-times. When comparing the results from CNTRL and EXPT the impact of coupled air-sea interactions (as a result of the atmosphere and ocean model coupling for EXPT) is suggested. It seems plausible that the ARW boundary-layer thermodynamic fluxes from the respective SST boundary conditions have propagated into the free atmosphere and have contributed to the respective CPS assessments. As a result, we may deduce that the time-scales for the troposphere response to the SST variability are on the order of 48-hours and are also dependent on the relative intensity for TC Ike (see Figure 5). However, the experiments conducted in this study do not permit us to diagnose whether the TC intensity variability (at longer forecast lead-times) is a result of the troposphere thermodynamic variability or vice versa.

4.4. Tropical Cyclone Size Implications

[35] The ROC, as a function of forecast lead-time for each TC Ike (2008) experiment, is provided in Figure 7. Once again each experiment is color-coded in accordance with Figure 1 and similar to Figure 5 the differences between CNTRL and EXPT are provided by the black bars. The ROC uncertainty at 24-hour lead-time increases as TC Ike encounters land (green points) and subsequently moves over the SSTs in the Gulf of Mexico (blue points). The variability for the ROC is on the order of the grid scale thus making it impossible to deduce whether the SST boundary condition is responsible or whether the ROC estimated by the TC diagnosis algorithm is an artifact of the grid resolution used in this study.

[36] The ROC, the RMW (not shown), and thus the IKE (not shown) variability for CNTRL and EXPT continues to increase at forecast lead times of 48- and 72-hours, and particularly when the V_{\max} intensity increases. The uncertainty related to the position of the TC (see Figure 4) leads to different interactions with both land (green points) and evolving 3-dimensional oceanic features for EXPT (blue points). The implications for both the TC intensity and the atmosphere and ocean boundary layers, resulting from the trajectories that TCs travel across such oceanic features, has been discussed by Yablonsky and Ginis [2011]. Similar to the CPS results presented in the previous section, it seems impossible to determine exactly whether the variability and uncertainty for the ROC, the RMW, and thus the IKE is a deterministic feature of the respective SST boundary conditions or a combination of the non-linear feedbacks related to the interaction of the ARW boundary-layer parameterization with the respective CNTRL and EXPT SST boundary conditions.

4.5. Synoptic-Scale and Larger Scale Environment Implications

[37] For completeness, we evaluate the synoptic-scale environment and the uncertainty associated with the

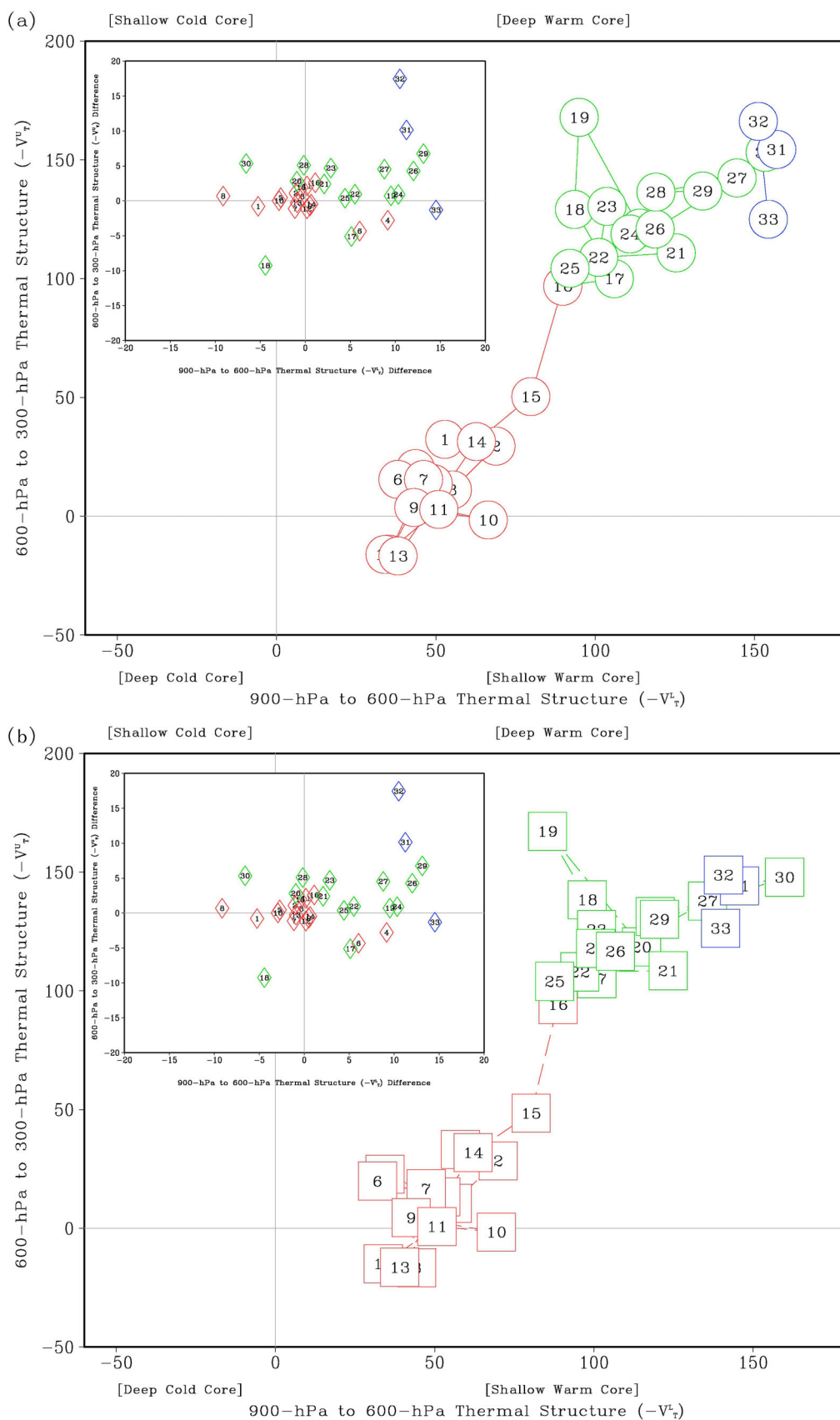


Figure 6. Troposphere thermodynamic structure (e.g., $(-V_T^L)$ versus $(-V_T^U)$) CPS [Hart, 2003] analyses for the TC Ike (2008) CNTRL (top) and EXPT (bottom) experiments initialized on the dates indicated by the number corresponding to those in Figure 1 for (a, b) 24-hour, (c, d) 48-hour, and (e, f) 72-hour lead-times. The insets within each figure are the differences for $(-V_T^L)$ and $(-V_T^U)$ from the CNTRL and EXPT experiments for the respective forecast hour lead-time.

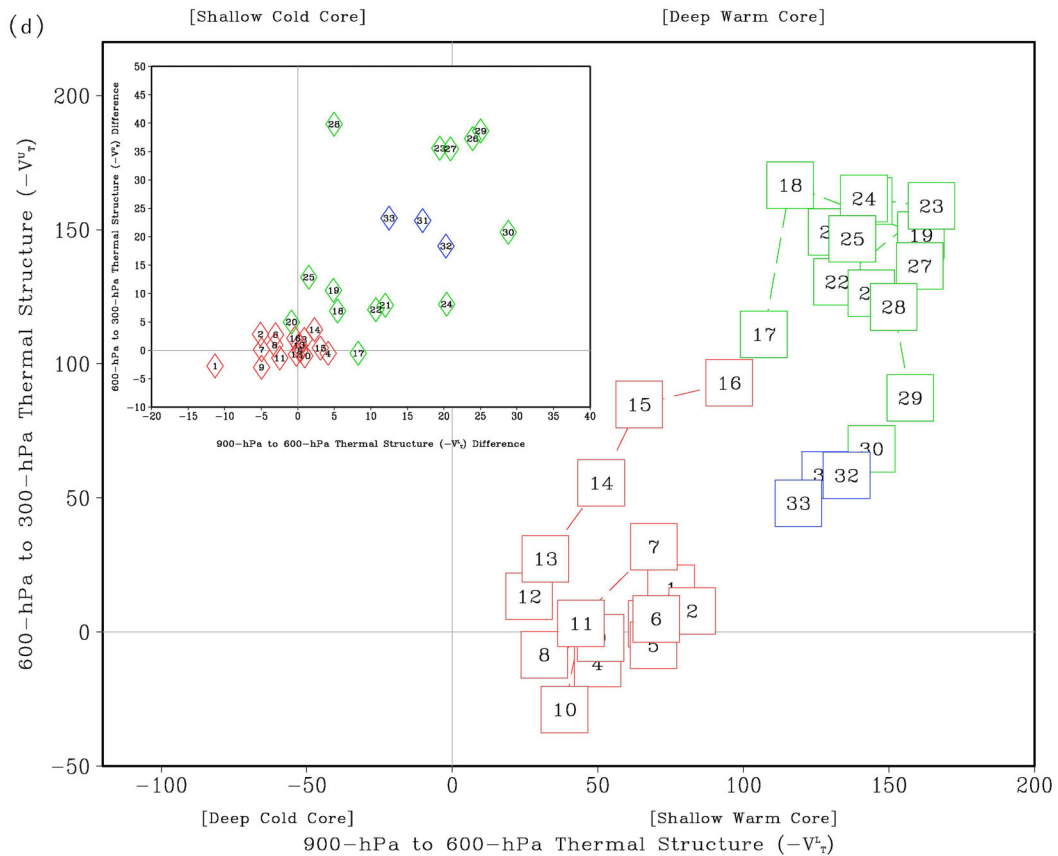
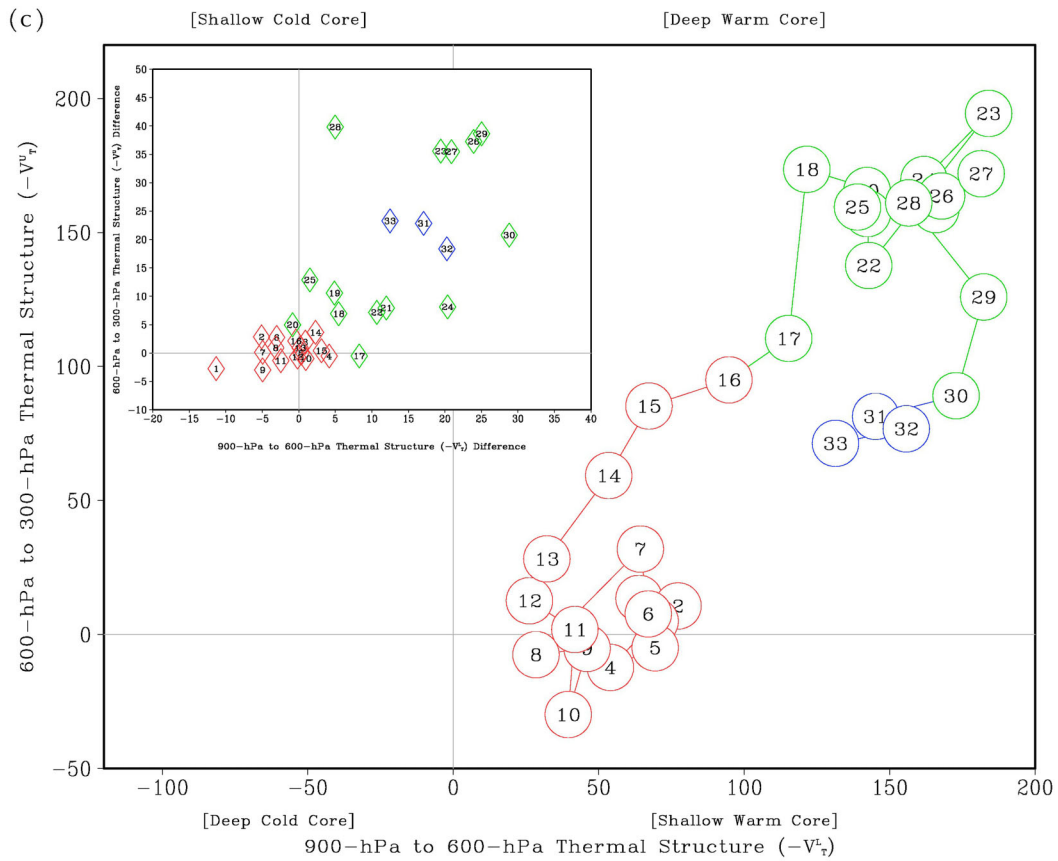


Figure 6. Continued.

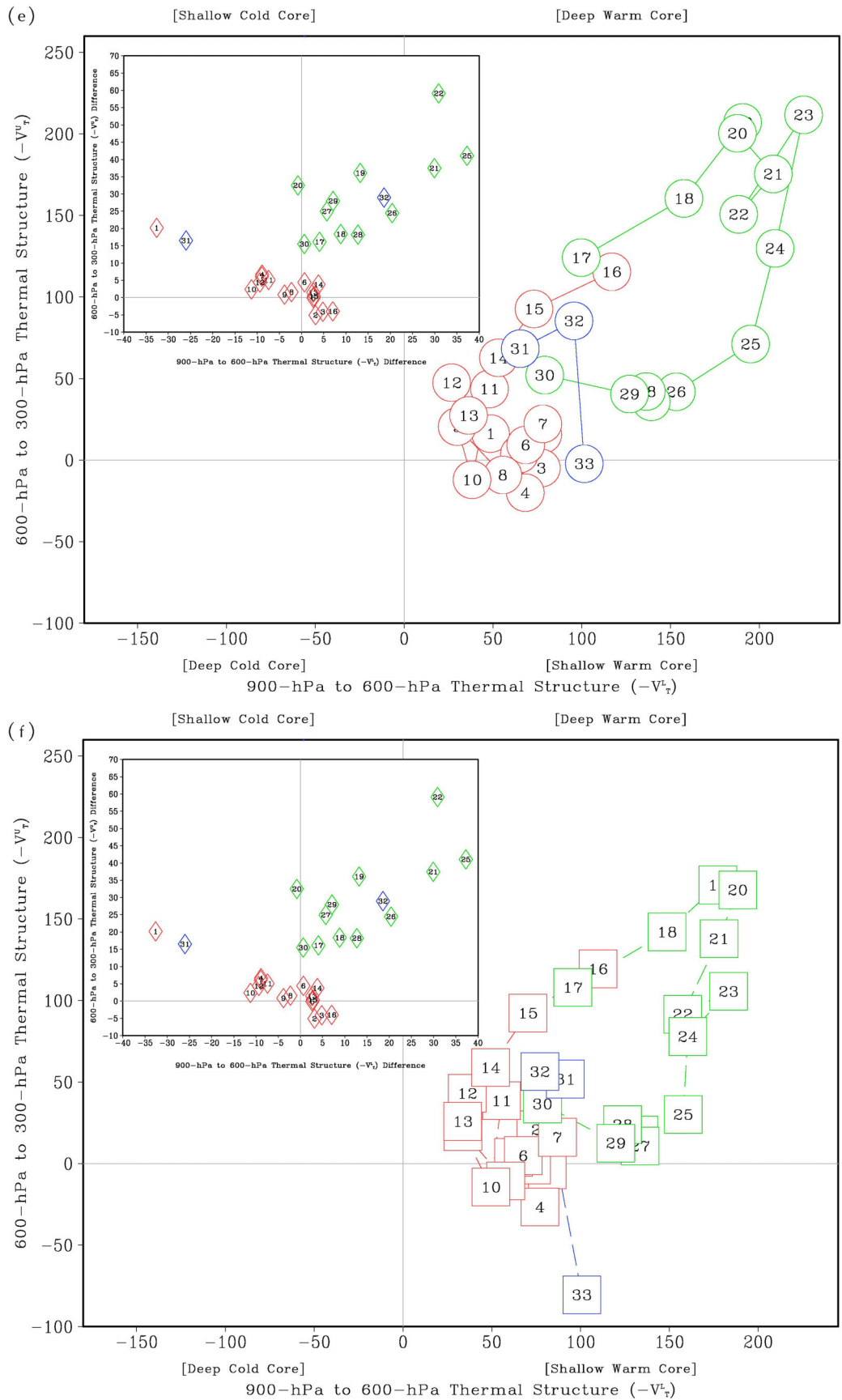


Figure 6. Continued.

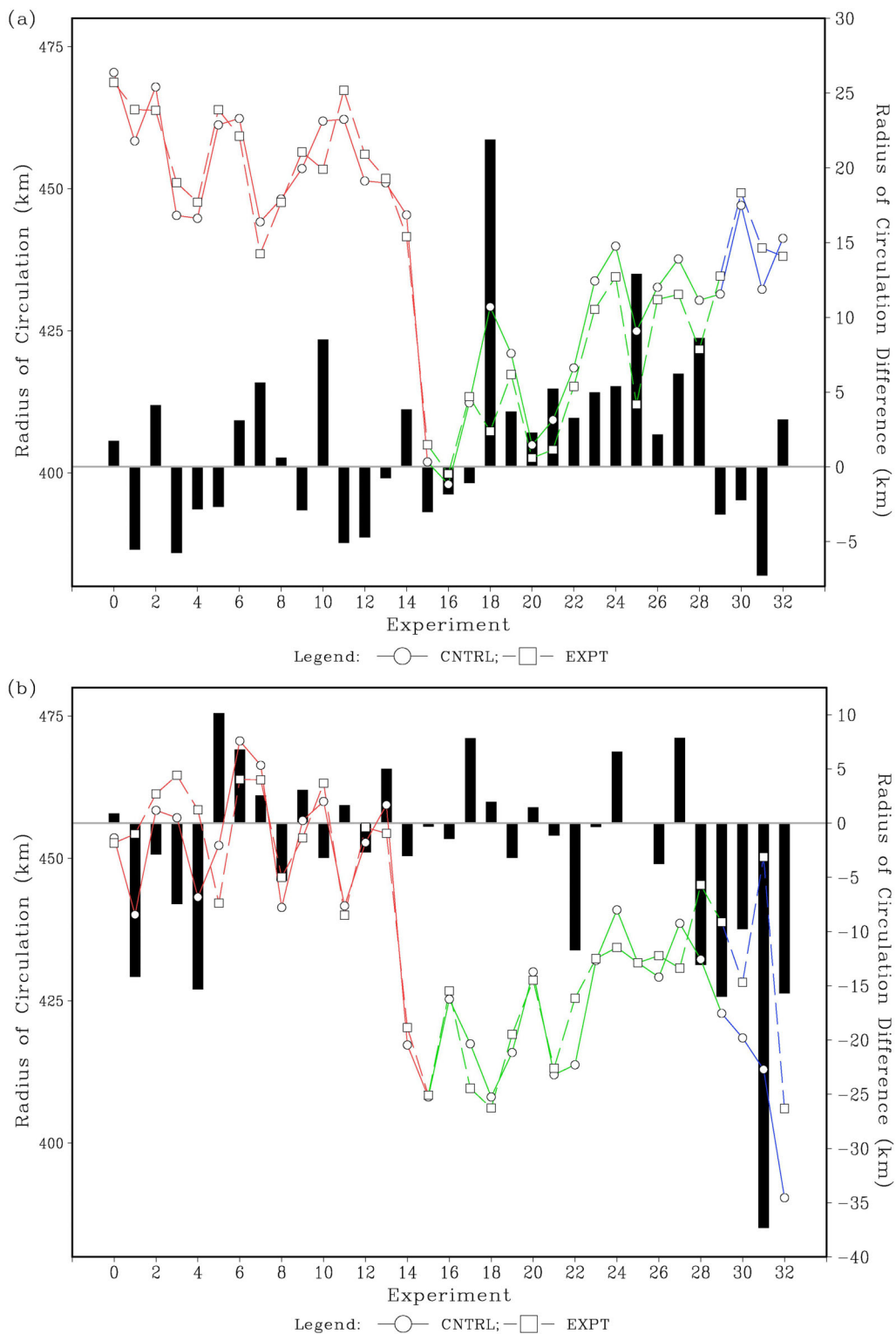


Figure 7. TC Ike (2008) ROC at (a) 24-hour, (b) 48-hour, and (c) 72-hour forecast lead-times for the experiment configurations denoted within the legend. The colors and the experiment numbers (along the x-axis) are identical to those illustrated in Figure 1. The black histogram bars indicate the difference between CNTRL and EXPT experiments (i.e., CNTRL – EXPT).

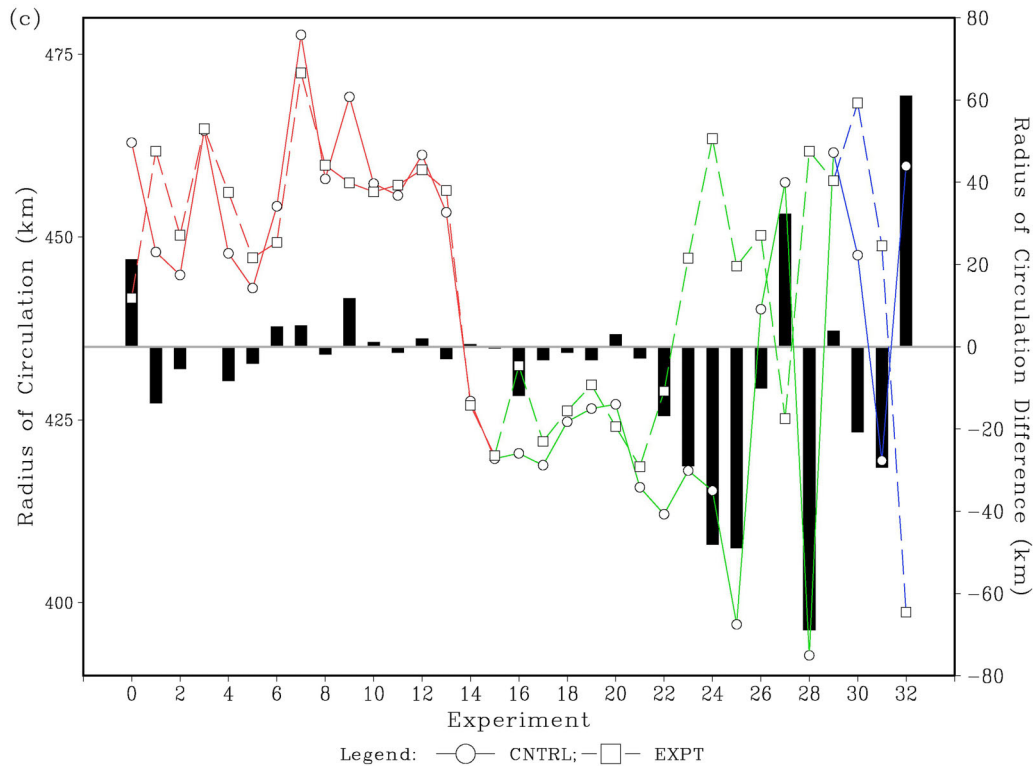


Figure 7. Continued.

SST boundary using the TC maximum potential intensity (MPI) and the genesis potential index (GPI) metrics defined in *Emanuel* [1986] and *Emanuel and Nolan* [2004], respectively. For the calculations of both the MPI and GPI metrics, a 600-km areal region relative to TC Ike (2008) is defined and all ARW grid points within this region and those over land are excluded from the MPI and GPI calculations. At all forecast lead-times evaluated in this study, the MPI and GPI differences for the large-scale (e.g., synoptic) environment are negligible. ARW domain mean thermodynamic soundings (not shown) and evaluations for both the large-scale shear and environmental steering vectors indicate that the forecast variability introduced by the SST boundary conditions remains at the scales of the TC vortex for forecast lead-times out to 72-hours.

[38] The experiments performed in this study, CNTRL and EXPT, demonstrate that the TC relative variables (namely intensity and structure) demonstrate a sensitivity to the SST boundary condition. The time-scales for the variability of the respective variables differ but remain coupled and thus mutually interactive. The larger (i.e., synoptic) scale variables do not appear to be as sensitive to the SST boundary condition at forecast lead-times up to 72-hours during the life-cycle of TC Ike (2008). These suggest that a static, high-resolution, and data assimilation derived ocean (i.e., SST) boundary condition (HYCOM) provides similar forecast skill for the environmental scales while introducing variability with respect to the TC track, intensity, and structure predictions. We are not implying that this will be or is the case for all TC events but true only for the TC Ike

(2008) experiments conducted in this study. Further evaluations and model configurations are required to determine whether there exists similar behavior for a larger sample of TC events. These topics remain the focus of future studies but are now viable using the coupled atmosphere-ocean model developed in the first part of this study. Finally, we are not implying that one experiment's result is superior to the other. Rather we are simply illustrating the sensitivity of the predicted variables to the SST boundary condition.

5. Conclusions and Discussion

[39] The intention of this study was the development of a coupled atmosphere-ocean model and a subsequent evaluation of the impact of the SST boundary condition on both the scales of the TC (e.g., track, intensity, and structure) and the larger (i.e., environmental) scales. The development of the respective coupled-model and algorithms to generate suitable (and balanced) ocean initial conditions is provided in Section 2. An evaluation of the experiments conducted from static SST boundary conditions and those from the coupled-model are provided in Section 4. We find that during the life-cycle of TC Ike, 0000 UTC 03 September through 0000 UTC 11 September 2008, the predicted variables at the scales of the TC demonstrate a sensitivity to the SST boundary condition, particularly at 48- to 72-hour forecast lead-times. It is also found, however, that the larger (synoptic) scale predicted variables remain largely impervious to the SST boundary condition variability at forecast lead-times up to 72-hours.

[40] We feel that the results from this study demonstrate and suggest some important considerations for TC modeling experiments. The first is that the inclusion of an *active* ocean (e.g., coupled atmosphere-ocean model) boundary condition alone does not guarantee an improved forecast for the TC as has been hypothesized. Although this study examined the life-cycle of a single TC, similar studies examining the variance and uncertainties introduced by SST boundary conditions for different TC case studies [Winterbottom, 2010] further substantiate this conclusion. We note that the coupled-model behaves as expected by modulating (and cooling) the SST in the wake of TC Ike (2008). However, the larger scale variables do not exhibit much variability amongst the CNTRL and EXPT experiments. Based on the computational cost required to run high-resolution coupled atmosphere-ocean (and eventually other geophysical) models, determining methodologies for evolving the SST boundary condition beneath the TC, rather than across the entire NWP model grid, may be a fruitful avenue of future research.

[41] The second consideration for TC modeling experiments relates to the respective atmosphere and ocean model initial conditions. Much of the work from recent years has been focused on providing optimal initial conditions for the atmospheric model, in particular for the initial conditions defining the TC [Kurihara et al., 1993, 1995; Zou and Xiao, 2000; Xiao et al., 2000, 2006]. More recent methodologies have been developed to emulate a similar effort for the ocean model initial state [Falkovich et al., 2005; Chassignet et al., 2007; Yablonsky and Ginis, 2008; Halliwell et al., 2008]. The results from the experiments conducted in this study suggest that the TC forecast *does* have a dependency on the SST boundary condition. However, we are left pondering whether a fully coupled-model is actually imperative to improving short-term (e.g., 72-hour) TC predictions or whether a *better* (i.e., more accurate) initial condition for the oceanic initial state would provide similar improvements while simultaneously reducing the computational expense. This conclusion results from the uncertainty for the exact temporal-scales at which the atmosphere becomes sensitive to the coupled-model produced SSTs (i.e., EXPT) versus the temporal variability induced by a static (i.e., CNTRL) SST boundary condition. Diagnosing just how much the SST influences the simulated TC is complicated by the non-linear interactions between the SST boundary condition and the atmospheric model physics parameterizations and is thus not easily deduced using the forecast evaluation metrics designed for this study.

[42] In conclusion, simply incorporating an evolving SST boundary condition versus the use of static SST boundary condition does not appear to be a stand-alone mechanism for improving the NWP model forecasts during the life cycle of TC Ike (2008). For most experiments, at all forecast lead-times, the track predictions are largely not impacted by the SST boundary condition (see Figure 4). This is consistent with the findings of Goerss [2006] and the fact that the

larger-scale environment remains largely un-modulated amongst the different experiments. Conversely, the intensity forecasts diverge as the lead-time increases and the coupled-model (EXPT) intensity forecasts are generally weaker than those of the static SST experiments (CNTRL). This characteristic is consistent with the intent of the coupled-model SST boundary condition – to respond in time to the forcing provided by the atmosphere (i.e., TC). The results presented here for TC Ike (2008), suggest that the skill of the coupled-model may depend (at least in part) upon the accuracy of the atmospheric forcing (e.g., the initial conditions). This hypothesis will be investigated further in subsequent studies using a data-assimilative coupled atmosphere-ocean prediction system.

[43] **Acknowledgments.** The research in this manuscript benefited from numerous discussions with Robert E. Hart, Carol Anne Clayson, and Qingnong N. Xiao. The authors would like to acknowledge the careful critiques of two anonymous reviewers as well as the informal reviews provided by Phillip J. Pegion and Jeffrey S. Whitaker.

References

- Bao, J.-W., J. M. Wilczak, J.-K. Choi, and L. H. Kantha (2000), Numerical simulations of air–sea interaction under high wind conditions using a coupled model: A study of hurricane development, *Mon. Weather Rev.*, *128*, 2190–2210, doi:10.1175/1520-0493(2000)128<2190:NSOASI>2.0.CO;2.
- Bender, M. A., and I. Ginis (2000), Real-case simulations of hurricane–ocean interaction using a high-resolution coupled model: Effects on hurricane intensity, *Mon. Weather Rev.*, *128*, 917–946, doi:10.1175/1520-0493(2000)128<0917:RCSOHO>2.0.CO;2.
- Berg, R. (2009), Tropical cyclone report: Hurricane Ike, 1 September – 14 September, 2008, TPC-NHC Rep. AL092008, 55 pp., NOAA, Silver Spring, Md.
- Bleck, R. (2002), An oceanic general circulation model framed in the hybrid isopycnic-Cartesian coordinates, *Ocean Modell.*, *4*, 55–88, doi:10.1016/S1463-5003(01)00012-9.
- Blumberg, A. F., and G. L. Mellor (1987), A description of a three-dimensional coastal ocean circulation model, in *Three Dimensional Ocean Models*, edited by N. Heaps, pp. 1–16, AGU, Washington, D. C., doi:10.1029/CO004p0001.
- Brooks, D. A. (1983), The wake of Hurricane Allen in the western Gulf of Mexico, *J. Phys. Oceanogr.*, *13*, 117–129, doi:10.1175/1520-0485(1983)013<0117:TWOHAI>2.0.CO;2.
- Chan, J. C. L., Y. Duan, and L. K. Shay (2001), Tropical cyclone intensity change from a simple ocean–atmosphere coupled model, *J. Atmos. Sci.*, *58*, 154–172, doi:10.1175/1520-0469(2001)058<0154:TCICFA>2.0.CO;2.
- Chassignet, E. P., L. T. Smith, G. R. Halliwell, and R. Bleck (2003), North Atlantic simulations within the Hybrid Coordinate Ocean Model (HYCOM): Impact of vertical coordinate choice, reference density, and thermobaricity, *J. Phys. Oceanogr.*, *33*, 2504–2526, doi:10.1175/1520-0485(2003)033<2504:NASWTH>2.0.CO;2.
- Chassignet, E. P., H. E. Hurlburt, O. M. Smedstad, G. R. Halliwell, P. J. Hogan, A. J. Wallcraft, and R. Bleck (2007), The HYCOM (HYbrid Coordinate Ocean Model) data assimilative system, *J. Mar. Syst.*, *65*, 60–83, doi:10.1016/j.jmarsys.2005.09.016.
- Chassignet, E. P., et al. (2009), US GODAE: Global Ocean Prediction with the HYbrid Coordinate Ocean Model (HYCOM), *Oceanography*, *22*, 64–75, doi:10.5670/oceanog.2009.39.
- Chen, S. S., W. Zhao, M. A. Donelan, J. F. Price, and E. J. Walsh (2007), The CBLAST-hurricane program and the next-generation fully coupled atmosphere–wave–Ocean models for hurricane research and prediction, *Bull. Am. Meteorol. Soc.*, *88*, 311–317, doi:10.1175/BAMS-88-3-311.
- Cione, J. J., and E. W. Uhlhorn (2003), Sea surface temperature variability in hurricanes: Implications with respect to intensity change, *Mon. Weather Rev.*, *131*, 1783–1796, doi:10.1175//2562.1.
- Demuth, J. L., M. DeMaria, and J. A. Knaff (2006), Improvement of advanced microwave sounding unit tropical cyclone intensity and

- size estimation algorithms, *J. Appl. Meteorol. Climatol.*, *45*, 1573–1581, doi:10.1175/JAM2429.1.
- Dong, K., and C. J. Neumann (1986), The relationship between tropical cyclone motion and environmental geostrophic flows, *Mon. Weather Rev.*, *114*, 115–122, doi:10.1175/1520-0493(1986)114<0115:TRBTM>2.0.CO;2.
- Elsberry, R. L. (1995), Tropical cyclone motion, in *Global Perspectives on Tropical Cyclones, Rep. TD-693*, pp. 106–191, World Meteorol. Org., Geneva, Switzerland.
- Emanuel, K. A. (1986), An air–sea interaction theory for tropical cyclones. Part I: Steady state maintenance, *J. Atmos. Sci.*, *43*, 585–605, doi:10.1175/1520-0469(1986)043<0585:AASITF>2.0.CO;2.
- Emanuel, K. A., and D. S. Nolan (2004), Tropical cyclone activity and global climate. Preprints, in *26th Conf. on Hurricanes and Tropical Meteorology*, pp. 240–241, Am. Meteorol. Soc., Boston, Mass.
- Falkovich, A., I. Ginis, and S. Lord (2005), Ocean data assimilation and initialization procedure for the Coupled GFDL/URI Hurricane Prediction System, *J. Atmos. Oceanic Technol.*, *22*, 1918–1932, doi:10.1175/JTECH1810.1.
- Goerss, J. S. (2006), Prediction of tropical cyclone track forecast error for Hurricanes Katrina, Rita, and Wilma, paper presented at 27th Conference on Hurricanes and Tropical Meteorology, Am. Meteorol. Soc., Monterey, Calif.
- Halliwell, G. R. (2004), Evaluation of vertical coordinates and vertical mixing algorithms in the HYbrid Coordinate Ocean Model (HYCOM), *Ocean Modell.*, *7*, 285–322, doi:10.1016/j.ocemod.2003.10.002.
- Halliwell, G. R., L. K. Shay, S. D. Jacob, O. M. Smedstad, and E. W. Uhlhorn (2008), Improving ocean model initialization for coupled tropical cyclone forecast using GODAE nowcasts, *Mon. Weather Rev.*, *136*, 2576–2591, doi:10.1175/2007MWR2154.1.
- Hart, R. E. (2003), A cyclone phase space derived from thermal wind and thermal asymmetry, *Mon. Weather Rev.*, *131*, 585–616, doi:10.1175/1520-0493(2003)131<0585:ACPSDF>2.0.CO;2.
- Hong, X., S. W. Chang, S. Raman, L. K. Shay, and R. Hodur (2000), The interaction between Hurricane Opal (1995) and a warm core ring in the Gulf of Mexico, *Mon. Weather Rev.*, *128*, 1347–1365, doi:10.1175/1520-0493(2000)128<1347:TIBHOA>2.0.CO;2.
- Kara, A. B., P. A. Rochford, and H. E. Hurlburt (2000), Efficient and accurate bulk parameterizations of air–sea fluxes for use in general circulation models, *J. Atmos. Oceanic Technol.*, *17*, 1421–1438, doi:10.1175/1520-0426(2000)017<1421:EAABPO>2.0.CO;2.
- Kimball, S. K., and M. S. Mulekar (2004), A 15-year climatology of North Atlantic tropical cyclones. Part I: Size parameters, *J. Clim.*, *17*, 3555–3575, doi:10.1175/1520-0442(2004)017<3555:AYCONA>2.0.CO;2.
- Kurihara, Y., M. A. Bender, and R. J. Ross (1993), An initialization scheme of hurricane models by vortex specification, *Mon. Weather Rev.*, *121*, 2030–2045, doi:10.1175/1520-0493(1993)121<2030:AISOHM>2.0.CO;2.
- Kurihara, Y., M. A. Bender, R. E. Tuleya, and R. J. Ross (1995), Improvements in the GFDL hurricane prediction system, *Mon. Weather Rev.*, *123*, 2791–2801, doi:10.1175/1520-0493(1995)123<2791:IITGHP>2.0.CO;2.
- Liu, K. S., and J. C. L. Chan (1999), Size of tropical cyclones as inferred from ERS-1 and ERS-2 data, *Mon. Weather Rev.*, *127*, 2992–3001, doi:10.1175/1520-0493(1999)127<2992:SOTCAI>2.0.CO;2.
- Lord, S. J. (1991), A bogusing system for vortex circulations in the National Meteorological Center global forecast model, in *19th Conference on Hurricanes and Tropical Meteorology*, pp. 328–330, Am. Meteorol. Soc., Boston, Mass.
- Marchok, T. P. (2002), How the NCEP tropical cyclone tracker works, in *25th Conference on Hurricanes and Tropical Meteorology*, pp. 21–22, Am. Meteorol. Soc., Boston, Mass.
- Moon, I.-J., I. Ginis, and T. Hara (2004), Effect of surface waves on air–sea momentum exchange. Part II: Behavior of drag coefficient under tropical cyclones, *J. Atmos. Sci.*, *61*, 2334–2348, doi:10.1175/1520-0469(2004)061<2334:EOSWOA>2.0.CO;2.
- Nolan, D. S., J. A. Zhang, and D. P. Stern (2009a), Evaluation of planetary boundary layer parameterizations in tropical cyclones by comparison of in situ observations and high-resolution simulations of Hurricane Isabel (2003). Part I: Initialization, maximum winds, and the outer-core boundary layer, *Mon. Weather Rev.*, *137*, 3651–3674, doi:10.1175/2009MWR2785.1.
- Nolan, D. S., D. P. Stern, and J. A. Zhang (2009b), Evaluation of planetary boundary layer parameterizations in tropical cyclones by comparison of in situ observations and high-resolution simulations of Hurricane Isabel (2003). Part II: Inner-core boundary layer and eyewall structure, *Mon. Weather Rev.*, *137*, 3675–3698, doi:10.1175/2009MWR2786.1.
- Ooyama, K. V. (1990), A thermodynamic foundation for modeling the moist atmosphere, *J. Atmos. Sci.*, *47*, 2580–2593, doi:10.1175/1520-0469(1990)047<2580:ATFFMT>2.0.CO;2.
- Pike, A. C. (1985), Geopotential heights and thicknesses as predictors of Atlantic tropical cyclone motion and intensity, *Mon. Weather Rev.*, *113*, 931–940, doi:10.1175/1520-0493(1985)113<0931:GHATAP>2.0.CO;2.
- Powell, M. D., and T. A. Reinhold (2007), Tropical cyclone destructive potential by integrated kinetic energy, *Bull. Am. Meteorol. Soc.*, *88*, 513–526, doi:10.1175/BAMS-88-4-513.
- Powell, M. D., P. J. Vickery, and T. A. Reinhold (2003), Reduced drag coefficient for high wind speeds in tropical cyclones, *Nature*, *422*, 279–283, doi:10.1038/nature01481.
- Press, W. H., S. Teukolsky, W. Vetterling, and B. Flannery (1992), *Numerical Recipes in Fortran 77: The Art of Scientific Computing* 2nd ed., 933 pp., Cambridge Univ. Press, New York.
- Price, J. (1981), Upper ocean response to a hurricane, *J. Phys. Oceanogr.*, *11*, 153–175, doi:10.1175/1520-0485(1981)011<0153:UORTAH>2.0.CO;2.
- Shay, L. K., G. J. Goni, and P. G. Black (2000), Effects of a warm oceanic feature on Hurricane Opal, *Mon. Weather Rev.*, *128*, 1366–1383, doi:10.1175/1520-0493(2000)128<1366:EOAWOF>2.0.CO;2.
- Skamarock, W. C., J. B. Klemp, J. Dudhia, D. O. Gill, D. M. Barker, W. Wang, and J. G. Powers (2005), A description of the Advanced Research WRF Version 2, *Tech. Note NCAR/TN-468+STR*, 88 pp., Natl. Cent. for Atmos. Res., Boulder, Colo.
- Tolman, H. L. (1999), User manual and system documentation of WAVEWATCH-III version 1, *Tech. Note 166*, 110 pp., NOAA, Silver Spring, Md.
- Velden, C. S., and L. M. Leslie (1991), The basic relationship between tropical cyclone intensity and the depth of the environmental steering layer in the Australian Region, *Weather Forecast.*, *6*, 244–253, doi:10.1175/1520-0434(1991)006<0244:TBRBTC>2.0.CO;2.
- Wicker, L. J., and W. C. Skamarock (2002), Time splitting methods for elastic models using forward time schemes, *Mon. Weather Rev.*, *130*, 2088–2097, doi:10.1175/1520-0493(2002)130<2088:TSMFEM>2.0.CO;2.
- Winterbottom, H. R. (2010), The development of a high-resolution coupled atmosphere–ocean model and applications toward understanding the limiting factors for tropical cyclone intensity prediction, PhD dissertation, 155 pp. Florida State Univ., Tallahassee, Fla.
- Xiao, Q., X. Zou, and B. Wang (2000), Initialization and simulation of a landfalling hurricane using a variational bogus data assimilation scheme, *Mon. Weather Rev.*, *128*, 2252–2269, doi:10.1175/1520-0493(2000)128<2252:IASOAL>2.0.CO;2.
- Xiao, Q., Y.-H. Kuo, Y. Zhang, D. M. Barker, and D.-J. Won (2006), A tropical cyclone bogus data assimilation scheme in the MM5 3D-var system and numerical experiments with typhoon Rusa (2002) near landfall, *J. Meteorol. Soc. Jpn.*, *84*, 671–689, doi:10.2151/jmsj.84.671.
- Yablonsky, R. M., and I. Ginis (2008), Improving the ocean Initialization of coupled hurricane–ocean models using feature-based data assimilation, *Mon. Weather Rev.*, *136*, 2592–2607, doi:10.1175/2007MWR2166.1.
- Yablonsky, R. M., and I. Ginis (2011), Impact of a warm ocean eddy’s circulation on hurricane-induced sea surface cooling with implications for hurricane intensity, *Mon. Weather Rev.*, in press.
- Zhang, J. A. (2010), Estimation of dissipative heating using low-level in situ aircraft observations in the hurricane boundary layer, *J. Atmos. Sci.*, *67*, 1853–1862, doi:10.1175/2010JAS3397.1.
- Zhang, J. A., W. M. Drennan, P. G. Black, and J. R. French (2009), Turbulence structure of the hurricane boundary layer between the outer rainbands, *J. Atmos. Sci.*, *66*, 2455–2467, doi:10.1175/2009JAS2954.1.
- Zou, X., and Q. Xiao (2000), Studies on the initialization and simulation of a mature hurricane using a variational bogus data assimilation scheme, *J. Atmos. Sci.*, *57*, 836–860, doi:10.1175/1520-0469(2000)057<0836:SOTIAS>2.0.CO;2.

Corresponding author: H. R. Winterbottom, Cooperative Institute for Research in Environmental Studies, National Oceanic and Atmospheric Administration, Earth System Research Laboratory, 325 Broadway, Boulder, CO 80305-3328, USA. (henry.winterbottom@noaa.gov)